Bioorganic & Medicinal Chemistry Letters 21 (2011) 2419–2424

Contents lists available at ScienceDirect

Bioorganic & Medicinal Chemistry Letters

journal homepage: www.elsevier.com/locate/bmcl

Exploration of new scaffolds as potential MAO-A inhibitors using pharmacophore and 3D-QSAR based in silico screening

Suhas M. Shelke, Sharad H. Bhosale *, Radha Charan Dash, Mugdha R. Suryawanshi, Kakasaheb R. Mahadik

Department of Pharmaceutical Chemistry, Bharati Vidyapeeth Deemed University, Poona College of Pharmacy, Pune 411 038, Maharashtra, India

ARTICLE INFO

Article history:
Received 7 November 2010
Revised 25 January 2011
Accepted 16 February 2011
Available online 19 February 2011

Keywords:
MAO-A inhibitors
3D-QSAR
Docking
Pharmacophore
in silico screening

ABSTRACT

Monoamine oxidase-A (MAO-A) inhibitors are of particular importance in the treatment of depressive disorders. Herein described is pharmacophore generation and atom-based 3D-QSAR analysis of previously reported pyrrole based MAO-A inhibitors in order to get insight into their structural requirements responsible for high affinity. The best pharmacophore model generated consisted of four features DHHR: a hydrogen bond donor (D), two hydrophobic groups (H) and an aromatic ring (R). Based on model generated, a statistically valid 3D-QSAR with good predictability was developed. Derived pharmacophore was used as a query to search Zinc 'clean drug-like' database. Hits retrieved were passed progressively through filters like fitness score, predicted activity and docking scores. The survived hits present new scaffolds with a potential for MAO-A inhibition.

Monoamine oxidase (MAO) is a flavoenzyme localized on the outer mitochondrial membrane and present virtually in all tissues.[1] Based on the substrate and inhibitor specificities, two different isoforms of MAO are reported, MAO-A and MAO-B, which share 70% amino acid sequence identity. MAO-A is responsible for oxidative deamination of brain monoamines like epinephrine, nor-epinephrine, serotonin and is inhibited by clorgyline. On the other hand, MAO-B is responsible for metabolizing benzylamine, β-phenethylamine, dopamine and is inhibited by deprenyl.[2] Inhibition of MAO-A is of particular importance for the treatment of psychiatric disorders like depression, while that of MAO-B for treatment of neurological disorders such as Parkinsonism.[3] Recently it has been reported that elevated level of brain MAO-A is the primary monoamine lowering process in case of major depression.[4] This finding has rejuvenated the interest in the development of MAO-A inhibitors, as they can strike the root cause of depression.

Various highly active indole and pyrrole based MAO-A inhibitors had been previously reported, wherein many of the tested compounds showed several fold higher affinity towards the enzyme as compared to standard drugs (Fig. 1; Tables 1a and 1b).[5–8] We conceived it interesting to understand the structural features of these compounds responsible for their high affinity towards MAO-A, as it can be helpful for designing potent inhibitors of this enzyme. With this aim, a dataset of 82 compounds was selected for pharmacophore generation and atom-based 3D-QSAR analysis. Further, the obtained information was used to explore novel scaffolds with potential MAO-A inhibitor activity by performing in silico screening of Zinc 'clean drug-like' database[9] with pharmacophore model as a query. 3D-QSAR model was used to predict activity of the hits. Refinement of retrieved hits was accomplished by applying filters of fitness score, predicted activity and docking score. Hits passing sieving process could be looked at as prospective MAO-A inhibitors.

Pharmacophore and 3D-QSAR modeling was accomplished using Phase (Schrödinger, New York, USA).[10] Phase supports various ligand-based drug design approaches like pharmacophore perception, structure alignment, 3D-QSAR and database searching.[11] Docking studies were performed using Glide (Schrödinger, New York, USA).[12] Glide analyzes the spatial fit of the ligand to the defined active site as well as the favorability of ligand-receptor interactions by applying various filters using a grid-based method.[13]

Energy minimization of dataset structures was accomplished in Macromodel with OPLS 2005 force field.[14] Minimized structures were then imported in Phase and appropriate protonation states at physiological pH 7.2 ± 2.0 were assigned to them by Ligprep.[15] Various conformations of prepared structures were then generated using Confgen with OPLS 2001 force field using distance-dependent dielectric solvation treatment.[7] While defining pharma set, compounds with $pK_i \geqslant 2.0$ were designated as active, while those with $pK_i \leqslant -1.0$ as inactive. Default pharmacophore features in Phase include hydrogen bond acceptor (A), hydrogen bond donor (D), hydrophobic (H), negative (N), positive (P) and aromatic ring (R). These default definitions were used for development of pharmacophore model with the exception that hydrophobic feature definition in Phase was edited for considering phenyl ring

* Corresponding author. Tel.: +91 9011032735; fax: +91 20 25439383.
E-mail address: dr_shbhosale@rediffmail.com (S.H. Bhosale).

0960-894X/$ - see front matter © 2011 Elsevier Ltd. All rights reserved.
doi:10.1016/j.bmcl.2011.02.072

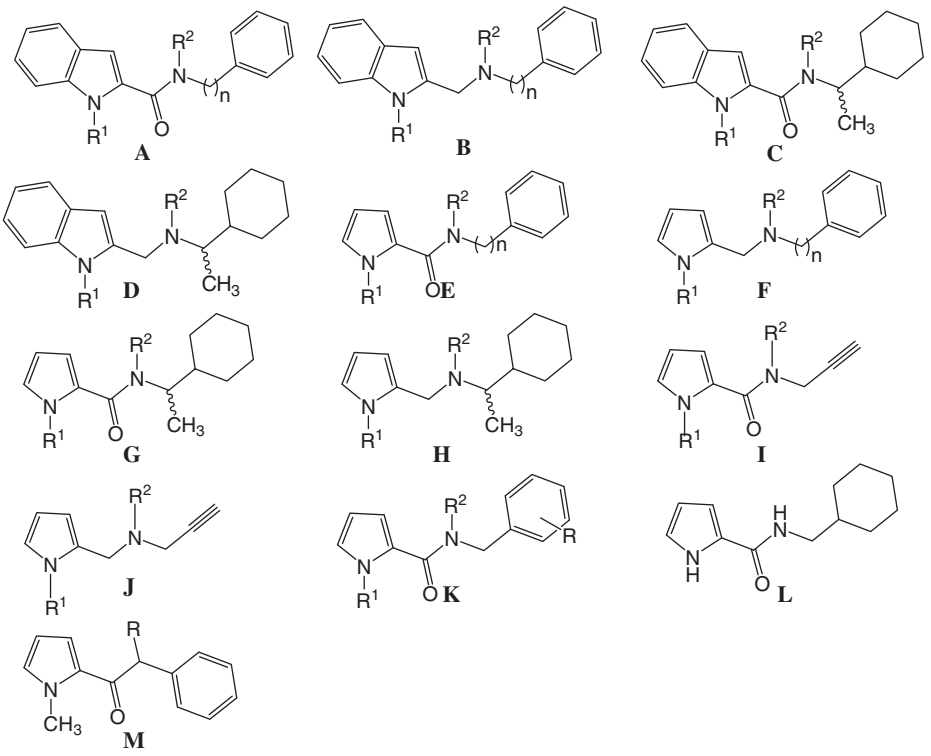

Figure 1. Core structures of various indole and pyrrole based MAO-A inhibitors included in study (for compounds, refer Tables 1a and 1b).

Table 1a
Dataset analyzed with experimental and predicted activities along with residual values[a,b]

#	Core	R^1	R^2	*n*	pK_i			#	Core	*	R^1	R^2	*n*	pK_i		
					Expt	Pred	Resd							Expt	Pred	Resd
1	A	H	H	0	0.886	0.79	0.096	31	C	*R*	H	CH_3		0.114	0.1	0.014
2	A	H	CH_3	0	2.456	2.47	−0.014	32	C	*S*	H	CH_3		1.921	1.97	−0.049
3	A	CH_3	H	0	−1.000	−1.12	0.120	33	C	*R*	CH_3	CH_3		0.155	0.06	0.095
4	A	CH_3	CH_3	0	1.824	1.86	−0.036	34	C	*S*	CH_3	CH_3		1.268	1.35	−0.082
5	A	H	H	1	1.523	1.47	0.053	**35**	**D**	***R***	**H**	**CH_3**		**2.000**	**1.33**	**0.670**
6	**A**	**H**	**CH_3**	**1**	**1.155**	**1.34**	**−0.185**	36	D	*S*	H	CH_3		1.222	1.15	0.072
7	A	CH_3	CH_3	1	2.222	2.15	0.072	37	D	*R*	CH_3	CH_3		−0.991	−1.01	0.019
8	**A**	**H**	**H**	**2**	**0.770**	**0.92**	**−0.150**	38	D	*S*	CH_3	CH_3		1.187	1.16	0.027
9	A	H	CH_3	2	2.398	2.31	0.088	39	E		H	H	0	0.398	0.29	0.108
10	A	CH_3	CH_3	2	2.187	2.16	0.027	40	E		H	H	1	0.602	0.43	0.172
11	A	H	H	3	2.301	2.15	0.151	41	E		H	CH_3	1	0.222	0.04	0.182
12	A	H	CH_3	3	3.036	3.2	−0.164	42	E		H	H	2	0.377	0.34	0.037
13	A	CH_3	H	3	1.000	1.05	−0.050	**43**	**E**		**H**	**CH_3**	**2**	**2.155**	**1.47**	**0.685**
14	**A**	**CH_3**	**CH_3**	**3**	**1.357**	**1.2**	**0.157**	44	E		H	H	3	0.155	0.19	−0.035
15	A	H	H	4	−0.342	−0.31	−0.032	45	E		H	CH_3	3	1.398	1.18	0.218
16	A	H	CH_3	4	−1.000	−1.01	0.010	46	E		H	H	4	1.260	1.08	0.180
17	**A**	**CH_3**	**CH_3**	**4**	**0.000**	**0.47**	**−0.470**	47	E		H	C H_3	4	1.046	0.94	0.106
18	B	H	H	0	−1.000	−0.55	−0.450	**48**	**F**		**H**	**H**	**1**	**0.456**	**0.53**	**−0.074**
19	B	H	CH_3	0	2.000	1.66	0.340	49	F		H	CH_3	1	−0.544	0.03	−0.574
20	B	CH_3	H	0	2.000	2.02	−0.020	50	F		CH_3	CH_3	1	0.824	0.66	0.164
21	B	CH_3	CH_3	0	2.222	2.33	−0.108	51	F		H	H	2	1.699	1.72	−0.021
22	B	H	H	1	−0.322	−0.51	0.188	52	F		H	CH_3	2	1.301	1.32	−0.019
23	B	H	CH_3	1	1.222	1.13	0.092	53	F		H	CH_3	3	1.301	1.33	−0.029
24	B	CH_3	CH_3	1	−0.857	−0.77	−0.087	**54**	**F**		**H**	**CH_3**	**4**	**1.000**	**0.82**	**0.180**
25	B	H	H	2	−0.204	−0.21	0.006	55	G	*R*	H	H		0.585	0.61	−0.025
26	B	H	CH_3	2	3.000	3.27	−0.270	56	G	*S*	H	H		0.481	0.43	0.051
27	B	CH_3	CH_3	2	2.155	2.38	−0.225	57	G	*R*	H	CH_3		2.770	2.84	−0.070
28	B	H	CH_3	3	1.137	1.16	−0.023	58	G	*S*	H	CH_3		1.699	1.75	−0.051
29	**B**	**CH_3**	**CH_3**	**3**	**1.051**	**0.58**	**0.471**	59	H	*R*	H	CH_3		1.699	1.59	0.109
30	B	H	H	4	−1.000	−0.94	−0.060	60	I		H	H		0.638	0.67	−0.032
								61	I		H	CH_3		1.125	1.17	−0.045
								62	I		CH_3	CH_3		0.081	0.15	−0.069
								63	J		H	CH_3		2.268	1.82	0.448
								64	J		CH_3	CH_3		0.357	0.54	−0.183

[a] Dataset entries for test set are in bold.
[b] For core, refer Figure 1.
* Stereochemistry.

Table 1b
Analyzed dataset with experimental and predicted activities[a,b]

#	Core	*	R^1	R^2	R	pK_i		
						Expt	Pred	Resd
65	**K**		**CH_3**	**H**	**H**	**0.585**	**0.4**	**0.185**
66	K		CH_3	CH_3	H	0.268	0.32	−0.052
67	K		H	H	4-F	0.143	0.31	−0.167
68	K		CH_3	H	4-F	0.398	0.26	0.138
69	**K**		**CH_3**	**CH_3**	**4-F**	**0.444**	**0.3**	**0.144**
70	K		H	H	3-F	0.469	0.52	−0.051
71	K		CH_3	H	3-F	0.699	0.6	0.099
72	K		CH_3	CH_3	3-F	0.009	0.11	−0.101
73	K		H	H	2-F	0.398	0.57	−0.172
74	K		CH_3	H	2-F	0.229	0.20	0.029
75	K		CH_3	CH_3	2-F	0.745	0.72	0.025
76	**L**					**0.301**	**0.27**	**0.031**
77	**M**	**R**			**C_4H_8N–**	**2.456**	**1.66**	**0.796**
78	**M**	S			**C_4H_8N**	**2.022**	**1.63**	**0.392**
79	M	R			$C_5H_{10}N$–	2.000	2.04	−0.040
80	M	S			$C_5H_{10}N$–	1.000	1.05	−0.050
81	M	R			C_4H_8NS–	1.119	1.22	−0.101
82	**M**	S			**C_4H_8NS–**	**1.086**	**1.04**	**0.046**

[a] Dataset entries for test set are in bold.
[b] For core, refer Figure 1.
* Stereochemistry.

as a hydrophobic group. For finding common pharmacophore, maximum number of sites was set to 6 and minimum to 3. Final box size of pharmacophore was adjusted to 2 Å. Active and inactive molecules were then scored for a given pharmacophore using default weights of scoring parameters. Top ranking hypotheses were subjected to 3D-QSAR analysis for which grid spacing was 1 Å and maximum PLS factors 10. Based on variation in structure and biological activity, 67 molecules were assigned to training set and 15 molecules to test set.

For docking studies, crystal structure of MAO-A with clorgyline (MLG) (PDB ID: 1O5W) was used.[16] After making necessary corrections to the structure of clorgyline and FAD, the protein was optimized for docking from its raw state employing Protein preparation wizard with OPLS 2005 force field for minimization.[17] Receptor gird generation with clorgyline as ligand was accomplished using Glide. Ligands were docked either in SP or XP mode with generation of maximum 5 poses. Best pose was selected on the basis of GlideScore which takes into account various favorable as well as unfavorable interactions of ligand with active site amino acids.

For the exploration of novel scaffolds with potential MAO-A inhibitory activity, an in silico screening of 1,40,000 compounds from Zinc 'clean drug-like' database[9] with derived pharmacophore model as a query was performed. The search criteria for compounds included in this database were: $x \log p \leqslant 5.0$, molecular weight in the range of 150–500, H-bond donor's $\leqslant 5$, H-bond acceptor's $\leqslant 10$. Molecules in the database were optimized with Ligprep[15] using OPLS 2005 force field along with generation of possible ionization states at physiological pH and likely tautomers.3D-QSAR model associated with the hypothesis predicted the biological activity of the hits. For the hits to be retrieved, matching of all the features in the query was made mandatory.

The generated pharmacophore hypotheses were evaluated on the basis of 'Survival' and 'Survival-inactive' scores.[10] The top scoring hypothesis DHRR.67 was selected as the best pharmacophore model for the present dataset of MAO-A inhibitors. DHHR.67 consisted of four features: hydrogen bond donor (D1), two hydrophobic groups (H2 and H4) and an aromatic ring (R6) (Fig. 2). Pharmacophore sites in DHRR.67 follow a spatial distribution analogous to a tetrahedron, with three features H, H and R forming its base and D at apex. Two H groups are coplanar and at the same distance of 6.64 Å from R. Feature closest to R is D, which is at a distance of 3.5 Å (Fig. 2). Thus, pharmacophore model postulates the involvement of hydrogen-bond formation along with aromatic and hydrophobic interaction with the enzyme. Based on the alignment of pharmacophore features, atom-based 3D-QSAR analysis was performed by PLS. Training set comprised of 67 compounds and test set of 15 compounds. Atom-based 3D-QSAR analysis yielded a statistically significant model which impressive predicted activity of test compounds. Biological activity predicted by 3D-QSAR for the present dataset is reported in Tables 1a and 1b. The PLS statistics for 3D-QSAR is shown in Table 2. Visual inspection of QSAR model revealed H-bond donor, hydrophobicity and electron-withdrawing effects as structural requirements critical

Table 2
Statistical values for 3D-QSAR model generated by PLS

Training set	Test set
$m = 6$	
$n = 67$	$n_T = 15$
$R^2 = 0.9785$	$Q^2 = 0.699$
SD = 0.1599	RMSE = 0.3944
$F = 454.7$, $P = 4.586$ e − 48	Pearson-$R = 0.9152$

m = number of PLS factors in the model; n = number of molecules in the training set; n_T = number of molecules in test set; R^2 = coefficient of determination; $Q^2 = R^2$ for test set; SD = standard deviation of regression; RMSE = root-mean squared error; F = variance ratio; P = statistical significance; Pearson-R = Pearson correlation coefficient.

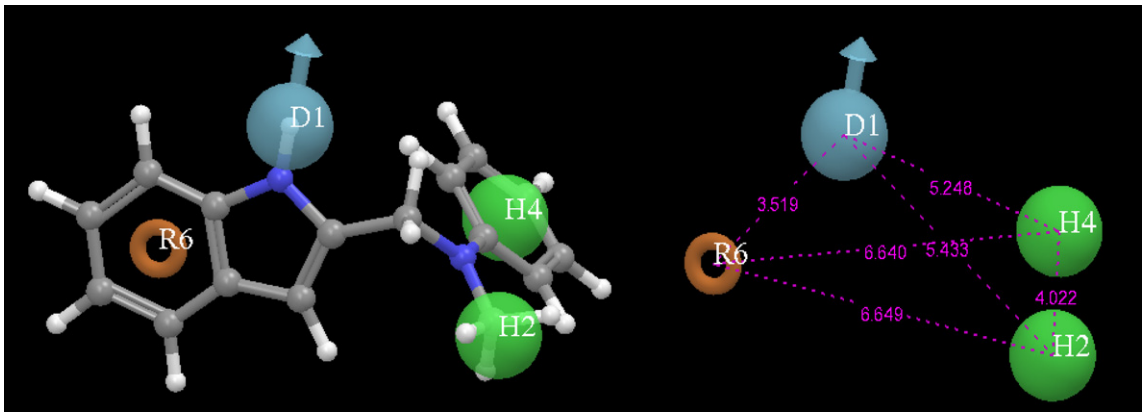

Figure 2. Generated pharmacophore model DHRR.67 aligned on best fit compound **19** (left) (light blue sphere: D; green sphere: H; orange torus: R); intersite distance in Å between pharmacophore features (right).

for activity; *H-bond donor*: presence of secondary pyrrole/indole nitrogen capable of acting as hydrogen bond donor seemed to have a favorable effect on activity. However, hydrogen bond donor in the side chain affected activity adversely (Fig. 3A); *Hydrophobicity*: hydrophobic group (methyl) at N-position of pyrrole/indole ring negatively correlated with activity, whereas as its presence on side-chain nitrogen had a positive influence on activity (Fig. 3B); *Electron-withdrawing*: presence of electron-withdrawing carbonyl group exercised a favorable effect on the activity (Fig. 3C). The plot of predicted pK_i against experimental is depicted in Figure 4.

For evaluating the interaction of inhibitors with MAO-A, active compounds were docked with crystal structure of the enzyme using Glide XP docking.[12] Active compounds interacted with the active site amino acids of the enzyme through hydrogen bond formation, π–π stacking and hydrophobic interaction. Docked conformation of compound **12** is represented in Figure 5. Best scoring pose for active compounds clearly indicated following interactions with the enzyme: (i) placement of terminal aromatic/hydrophobic group of ligand in the hydrophobic pocket formed by Tyr 69, Leu 97, Ile 180, Phe 208, Val 210, Ile 325, Ile 335, Leu 337 and Phe 352 (ii) π–π stacking interaction of indole/pyrrole ring with Tyr 407 and Tyr 444 (iii) H-bond interaction where indole –NH– formed a bond with –C=O of Asn 181. As can be seen from Figure 6, results of docking study categorically underlined the importance of features involved in pharmacophore model DHHR.67; donor feature (D1) being involved in formation of H-bond, hydrophobic features (H2 and H4) involved in establishing hydrophobic interactions where as aromatic feature (R) responsible for π–π stacking with active site residues.

While finding matches to hypothesis DHRR.67, a pre-screen of Zinc 'clean drug-like database' was performed using database keys. This was done for rapidly filtering out majority of molecules that cannot match the required features. Pre-screen search returned 30,052 compounds with desired pharmacophore features. Next, various conformers of these hits were generated and searched comprehensively for matches to pharmacophore model to return 28,288 hits. Subsequently, hits with fitness score less than 60% were discarded to reduce their number to 1572. Fitness score reflects extent of matching of pharmacophore features in a particular molecule with that of the features in the reference model. Of these,

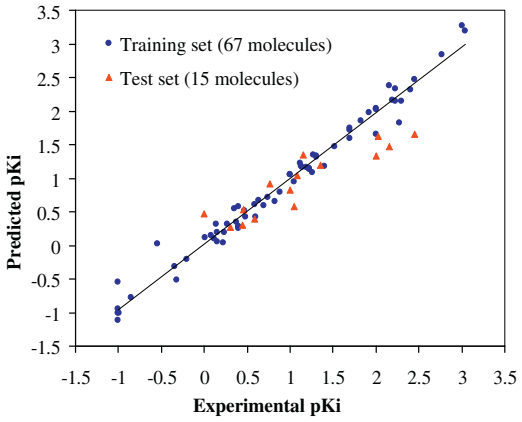

Figure 4. Scatter plot of predicted pK_i against experimental pK_i for training and test set compounds.

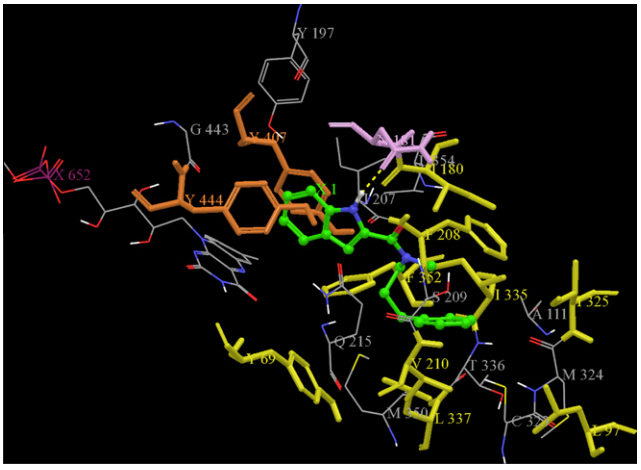

Figure 5. Glide XP docking of compound **12** (green) into active site of MAO-A (colour coding for residues; yellow: hydrophobic interaction, orange: π–π stacking, pink: H-bond formation).

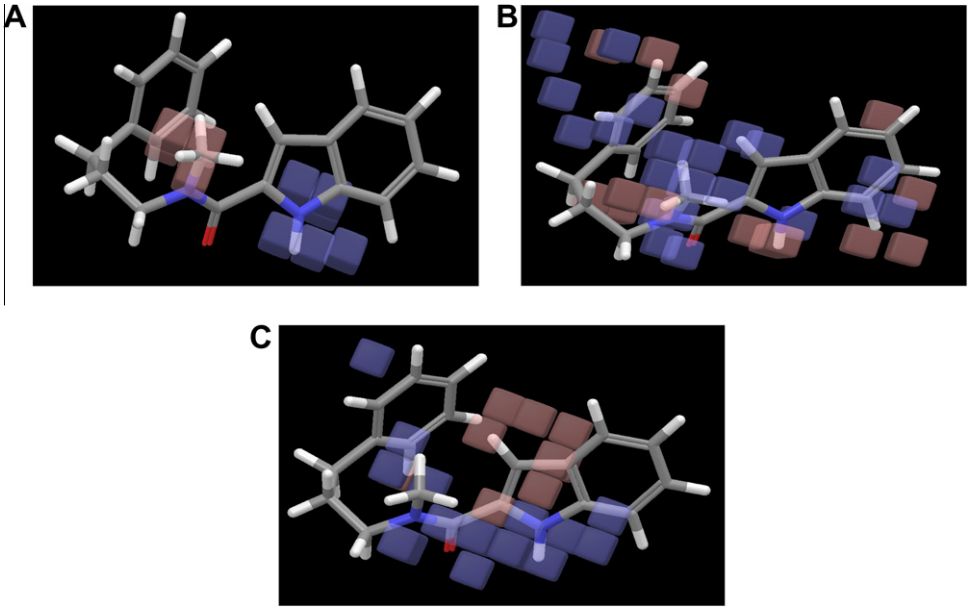

Figure 3. 3D-QSAR visualization for compound **12**; (A) H-bond donor, (B) Hydrophobic, (C) Electron-withdrawing (blue cubes: favorable influence on activity; red cubes: unfavorable influence on activity).

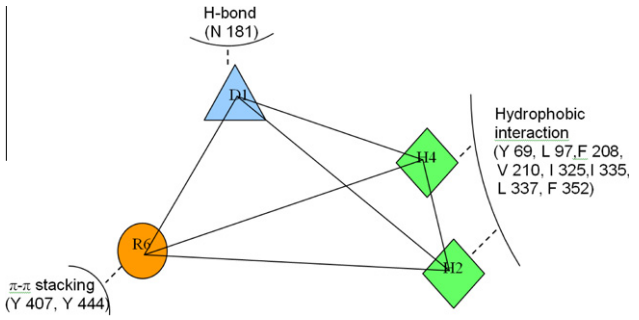

Figure 6. Representation of interaction between pharmacophore features and active site residues of MAO-A.

only those with predicted p$K_i \geqslant 1$ were retained to furnish 960 hits. Again, on the basis of docking score, sorting of hits was attempted in order to furnish only those hits which significantly interacted with the MAO-A. For this purpose, hits obtained in the previous step were subjected to Glide SP docking. 247 hits with SP *GlideScore* $\leqslant -8.0$ qualified for Glide XP docking, a computationally intensive more accurate docking algorithm. Finally, structurally varied 11 hits with XP *GlideScore* $\leqslant -8.0$, were considered as potential MAO-A inhibitors and are revealed in Figure 7.

The hits presented can factually be regarded as prospective MAO-A inhibitors since they fit satisfactorily generated pharmacophore model, have decent predicted pK_i for MAO-A inhibition along with impressive interaction with the enzyme as reflected from XP GlideScore.

The structurally diversity of retrieved hits emphasize the scaffold-hopping capability of DHRR.67, if used to mine the database of drug-like compounds. Further, experimental evaluation of these hits by enzymatic assays coupled together with computational methods can help in structural optimization of these hits. Additionally, application of other scaffold-hopping tools like Core-hopping (Schrödinger LLC, USA), Topomer Search, Scaffold and R-group search (BioPharmics LLC, USA) to these hits can effectively open an array of diverse potential MAO-A inhibitors, enabling their rational design.

To conclude, the present research work has carried out pharmacophore modeling and 3D-QSAR studies of some potent pyrrole based MAO-A inhibitors. The pharmacophore model DHHR.67 implicated the role of hydrogen bond donor (D1), hydrophobic features (H2 and H4) and an aromatic ring (R6) in biological activity. Docking studies of these compounds with crystal structure of MAO-A were also performed, which showed that active inhibitors interacted with the enzyme in three ways: H-bond formation, π–π stacking and hydrophobic interaction. Involvement of pharmacophoric features in interaction with the enzyme substantiates the developed pharmacophore model. For exploring new potential MAO-A inhibitors, DHRR.67 was used as a query for screening Zinc 'clean drug-like' database. The hits retrieved were passed through a series of hierarchical filters for enhancing the accuracy of in silico screening process. Finally, 11 hits recovered by scaffold-hopping offer structurally varied molecules as potential MAO-A inhibitors. Thus, pharmacophore model, 3D-QSAR study and in silico screening hits presented in this paper is hoped to be a primer towards the development of novel MAO-A inhibitors. Moreover, further use of contemporary experimental and computational techniques to data presented here may widen its scope and applicability.

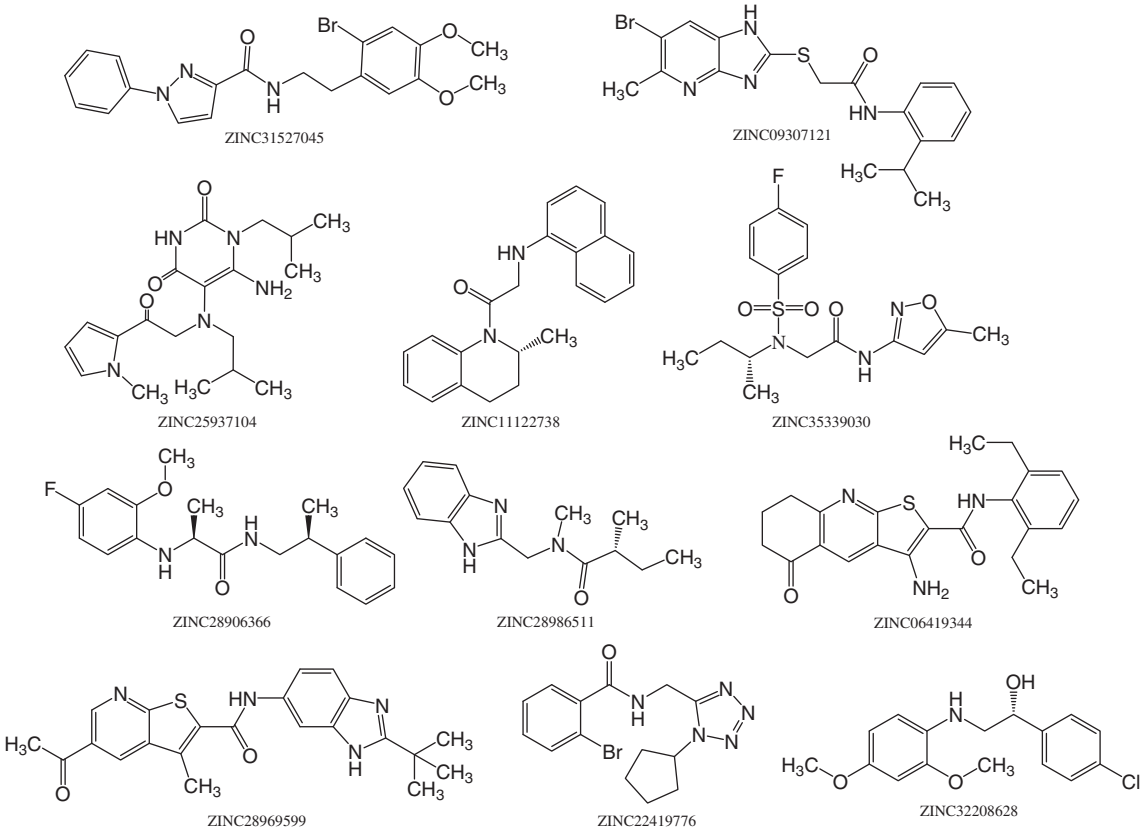

Figure 7. Structures of the final hits retrieved during in silico screening.

Acknowledgments

One of the authors (S.M.S.) is indebted to Council of Scientific and Industrial Research (CSIR), New Delhi, India, for awarding senior research fellowship. Authors wish to express their gratitude towards Dr. R. A. Joshi and Dr. (Mrs.) R. R. Joshi, National Chemical Laboratory, Pune, India, for their support.

Supplementary data

Supplementary data associated with this article can be found, in the online version, at doi:10.1016/j.bmcl.2011.02.072.

References and notes

1. Brunner, H. G.; Nelen, M. R.; Zandvoort, P.; Abeling, N.; Gennip, A. H.; Wolter, E. C.; Kuiper, M. A.; Roper, H. H.; Oust, B. A. *Am. J. Hum. Genet.* **1993**, *52*, 578.
2. Son, S.; Ma, J.; Kondou, Y.; Yoshimura, M.; Yamashita, E.; Tsukihara, T. *Proc. Natl. Acad. Sci. U.S.A.* **2008**, *105*, 5739.
3. Checkoway, H.; Franklin, G. M.; Costa-Mallen, P.; Smith-Weller, T.; Dilley, J.; Swansons, P. D.; Costa, L. G. *Neurology* **1998**, *50*, 1458.
4. Meyer, J. H.; Ginovart, N.; Boovariwala, A.; Sagrati, S.; Hussey, D.; Garcia, A.; Young, T.; Praschak-Rieder, N.; Wilson, A. A.; Houle, S. *Arch. Gen. Psychiatry* **2006**, *63*, 1209.
5. Silvestri, R.; Regina, G. L.; Martino, G. D.; Artico, M.; Befani, O.; Palumbo, M.; Agostinelli, E.; Turini, P. *J. Med. Chem.* **2003**, *46*, 917.
6. Santo, R. D.; Costi, R.; Roux, A.; Artico, M.; Befani, O.; Meninno, T.; Agostinelli, E.; Palmegiani, P.; Turini, P.; Cirilli, R.; Ferretti, R.; Gallinella, B.; Torre, F. L. *J. Med. Chem.* **2005**, *48*, 4220.
7. Regina, G. L.; Silvestri, R.; Artico, M.; Lavecchia, A.; Novellino, E.; Befani, O.; Turini, P.; Agostinelli, E. *J. Med. Chem.* **2007**, *50*, 922.
8. Regina, G. L.; Silvestri, R.; Gatti, V.; Lavecchia, A.; Novellino, E.; Befani, O.; Turini, P.; Agostinelli, E. *Bioorg. Med. Chem.* **2008**, *16*, 9729.
9. Irwin, J. J.; Shoichet, B. K. *J. Chem. Inf. Model* **2005**, *45*, 177.6.
10. Phase, version 3.1, Schrödinger, LLC, New York, NY, 2009. 7.
11. Dixon, S. L.; Smondyrev, A. M.; Knoll, E. H.; Rao, S. N.; Shaw, D. E.; Friesner, R. A. *J Comput. Aided Mol. Des.* **2006**, *20*, 647.8.
12. Glide, version 5.5, Schrödinger, LLC, New York, NY, 2009.9.
13. Friesner, R. A.; Banks, J. L.; Murphy, R. B.; Halgren, T. A.; Klicic, J. J.; Mainz, D. T.; Repasky, M. P.; Knoll, E. H.; Shelley, M. E.; Perry, J. K.; Shaw, D. E.; Francis, P.; Shenkin, P. S. *J. Med. Chem.* **2004**, *47*, 1739.10.
14. MacroModel, version 9.7, Schrödinger, LLC, New York, NY, 2009.11.
15. LigPrep, version 2.3, Schrödinger, LLC, New York, NY, 2009.12.
16. Ma, J.; Yoshimura, M.; Yamashita, E.; Nakagawa, A.; Ito, A.; Tsukihara, T. *J. Mol. Biol.* **2004**, *338*, 103. 13.
17. Schrödinger Suite 2009 Protein Preparation Wizard; Epik version 2.0; Impact version 5.5. Schrödinger, LLC, New York, NY, 2009.14.